Bulletin of the Geological Society of Malaysia, Volume 73, May 2022, pp. 1 - 12
DOI: https://doi.org/10.7186/bgsm73202201

Magnitude-rupture area scaling derived from global earthquakes of moderate to large sizes: Implications for seismic hazards in Indonesia

Tjipto Prastowo[1,2,*], Gandhis Putri Ayudia[1], Hilda Risanti[1]

[1] Physics Department, Universitas Negeri Surabaya, Surabaya 60231, Indonesia
[2] Centre for Earth Science Studies, Universitas Negeri Surabaya, Surabaya 60231, Indonesia
* Corresponding author email address: tjiptoprastowo@unesa.ac.id

Abstract: Earthquake size can be estimated using magnitude-rupture area scaling developed from modelled fault dimensions and measured moment magnitudes. In this study, a measure of a fault plane geometry was provided by rupture area A and the size scaled with moment magnitude M_w. Using global earthquakes datasets containing 90 events with varying magnitudes $4.45 \leq M_w \leq 9.20$ during years of 1960-2015, we classified the data into separate strike-slip, dip-slip (normal and reverse) and subduction-zone earthquakes. The study aims to search for reliable scaling used for magnitude prediction of earthquakes around the globe for each type of source mechanism. We found from the $M_w - A$ scaling proposed in this study that the magnitude for subduction events was likely to saturate to a maximum value possible $M_w \approx 9.3$ at rupture areas much larger than those for strike-slips and dip-slips. This suggests that rocks in the subduction-zone are able to accumulate high stress, implying large seismic energy release via strong ground motion when an earthquake occurs at the plate boundary. Taking into account cases under consideration that included intraplate-fault and subduction processes covering a wide range of magnitudes from moderate to large sizes, the results are relevant to Indonesian tectonic settings, where active crustal faults have been recently found throughout the country and in particular a future megathrust subduction-zone earthquake of $M_w \sim 9.0$ is possible to occur off the south coasts of Java Island, the most densely populated island in Indonesia. These potential seismic threats call for increasing awareness of disaster preparedness, particularly for local community in regions with a high level of vulnerability to tsunami and earthquake disasters. Therefore, a reliable earthquake early warning is of primary importance, which is best integrated into an existing tsunami early warning for maximum security from future seismic hazards.

Keywords: Moment magnitude, rupture area, magnitude-area scaling, fault dimensions, intraplate earthquake, subduction-zone earthquake

INTRODUCTION

Most of Indonesian territories are located in the regions of a relatively high seismicity (Cipta *et al*., 2016; Koulali *et al*., 2016; Koulali *et al*., 2017; Cummins, 2017; Watkinson & Hall, 2017; Lange *et al*., 2018; Gunawan & Widiyantoro, 2019; Salman *et al*., 2020) due to their positions at a triple junction of three major tectonic plates, that is, Eurasian, Indo-Australian and Pacific Plates (van Gorsel, 2018). These geological and tectonic settings lead to the potency for seismic threats possible to occur throughout the country induced by either moderate to large earthquakes from sources of active crustal faults (Irsyam *et al*., 2017) or potential megathrust events from complex subduction processes (Susilo *et al*., 2019; Triyoso *et al*., 2020; Widiyantoro *et al*., 2020). Figure 1 shows the geographical position of Indonesia with respect to the major tectonic plates. Sarawak and Sabah are part of Malaysian territories, which lie on Borneo Island, the second largest island in Indonesia.

In the context of vulnerability to and corresponding risk in the region of interest posed by such threats, this study examines estimates of earthquake strength in size based on a seismic scaling relation between earthquake size scaled with moment magnitude M_w and a causative fault plane parameter given by rupture area A (defined as the product of its length L and width W). The M_w scale is selected as it is widely known to be more accurate for all ranges of earthquake magnitudes compared to other magnitude scales. While many magnitude-area scaling relations follow previous work (Wells & Coppersmith, 1994; Hanks & Bakun, 2002; Shaw, 2009; Konstantinou, 2014), the $M_w - A$ scaling proposed in the current study is carried out for each faulting type of source mechanism, including for the subduction interface (Goda *et al*., 2016; Thingbaijam *et al*., 2017).

Fault dimensions are usually determined using appropriate finite-fault source models for particular cases worldwide (Yen & Ma, 2011; Wu *et al*., 2013; Murotani *et al*., 2015; Irikura *et al*., 2017) and those in Indonesia (Ratnasari *et al*., 2020; Salman *et al*., 2020). However, these studies have not yet discussed $M_w - A$ scaling applied to specific Indonesian settings with ground motions triggered by both intraplate and interplate events, leaving the problem being poorly understood for Indonesian contexts (Cummins, 2017;

0126-6187; 2637-109X / Published by the Geological Society of Malaysia.

Figure 1: A topographic map of Indonesia with ocean bathymetry surroundings, illustrating Indonesian territories at the triple junction of the three major plates. Sumatera Trench and Java Trench are part of the Sunda Arc. Insert shows the position of the Indonesian archipelago (red rectangle) with respect to the globe. This is made available using ArcGIS Online Basemaps at https://arcgis.com/home/group.html accessed at 23/8/21.

Irsyam *et al*., 2017). Concerning with this seismic hazard potential and associated efforts in disaster risk reduction, this study searches for empirical relations of the $M_w - A$ scaling appropriate for each source mechanism of ground shaking possible.

The followings are the saline points of previous work for the $M_w - A$ scaling. Wells & Coppersmith (1994) argued for their empirical relation, independent of epicenter distribution and fault type (not influenced by geographical positions, geological and tectonic settings). Focusing upon strike-slips, Hanks & Bakun (2002) related M_w to A based on stress drop if it was constant or variable and corresponding separate values of A. In contrast, Shaw (2009; 2013) claimed a single scaling for M_w and A, independent of stress drop variations but influenced by a fitting parameter from earthquake data.

Konstantinou (2014) discussed seismic activities in the Mediterranean mostly dominated by normal and strike-slip faulting with sizes of $M_w \sim 6.5$. Such moderate scales of faults have been observed for relevance to Indonesian settings in the sense that Indonesian earthquakes are characterised by fault movement releasing moderate to relatively large magnitudes of up to M_w 7.8 (Irsyam *et al*., 2017). Konstantinou (2014) brought Hanks & Bakun's ideas (2002) to incorporate fault area into source-scaling but did not include stress drop separation. However, as with the previous $M_w - A$ scaling relations, this scaling model did not separate the scaling law into different faulting types, making it difficult to apply to cases in Indonesia, where both active faults in the shallow crustal rocks and large-scale tectonic motions along the subduction-zone interface can be deadly earthquake potential.

All of the above models for the $M_w - A$ scaling have led to a $M_w \sim \log A$ scaling relation with no separation of source mechanism. Using databases of rupture models and the observed variations in magnitude-rupture area scaling properties for different faulting mechanisms, Thingbaijam *et al*. (2017) found substantial differences between their results and those of previous studies in that they obtained separate scaling of subduction-zone (interplate) events from the intraplate ones that are useful for seismic-tsunami hazard analysis. As the magnitude coverage of $5.4 \leq M_w \leq 9.2$ was used in their data for all faulting types (three of which were strike-slip, normal and reverse, and the one was subduction interface), their work is similar to the present study in terms of magnitude ranges covered (moderate to large sizes) and source-separation, for which the current results are examined in details. In addition, the results are also related to a future possibility for three seismic scenarios that may generate megathrust catastrophes of tsunami waves with a possible maximum height of ~ 20 m in the south-west coastal region of West Java and a spatially averaged height of ~ 5 m for the whole Java south coastal regions (Widiyantoro *et al.*, 2020).

Java Island is surrounded by the Indian Ocean in the south and the Java Sea in the north, with the mainland extends for almost 1,000 km long (from the west area near Sumatera Island to the east area near Bali Island) and 210 km wide (from the northern to the southern region). According to the Indonesian Bureau of Statistics (2020), Java is the most densely populated island in Indonesia with the number of its population occupies 56% of the total population. The southern regions of Java Island are relatively close to the

Java subduction zone, which is considered seismically active with two seismic segments (see Figure 2). These segments are locations where a potential megathrust earthquake may occur when the requirements meet (Widiyantoro *et al*., 2020). Regarding the growing number of Java population, Java Island is then considered prone to seismic hazards, including tsunami excitation of seismic origin.

Despite a number of large earthquakes followed by devastating tsunami waves striking some of coastal regions in Indonesia over the last two decades and subsequently considerable progress in understanding of tsunami and seismic hazard analysis, leading to programmes for disaster preparedness and disaster risk reduction in countries around the world (Satriano *et al*., 2011; Suppasri *et al*., 2015; Suppasri *et al*., 2017; Titov, 2021), seismic assessment and potential risks in Java particularly in the southern regions of Java remain poorly understood. A question like where the next megathrust earthquake may come (Marzocchi *et al*., 2016) is relatively easy to predict as it generally takes place on the plate boundary between two colliding plates. However, the worst is yet to come as the most likely probable maximum size remains questionable. This is of significance since earthquake magnitude is considered to be one of the source parameters important for estimate of tsunami potential. To this end, we here developed the $M_w - A$ scaling derived from global earthquake datasets for each faulting type. We then used the obtained scaling for the subduction case to estimate the size of a possible megathrust subduction-zone event off the south coasts of Java Island.

In order to describe global seismicity from which the $M_w - A$ scaling was obtained, we here provide a map of global earthquakes constructed by selecting some parameters made available by Incorporated Research Institutions for Seismology (IRIS) using an online IRIS Earthquake Browser (IEB). The selected earthquakes occurred worldwide during 1970-2020 with magnitudes greater than 6.5, which is considered to be large events, as seen in Figure 3. Notice that the map is not intended to show earthquake datasets used in the present

Figure 2: A map of Java Island, showing the Java Sea and the Indian Ocean as the north and south borders, respectively. The western and eastern Java segments are shown to the south of Java Island, occupying the Java subduction zone (adopted from Widiyantoro *et al*. (2020) for approximately the same geometry). Insert shows the position of Java Island among other islands in Indonesian territories. This is made available using ArcGIS Online Basemaps at https://arcgis.com/home/group.html accessed at 23/8/21.

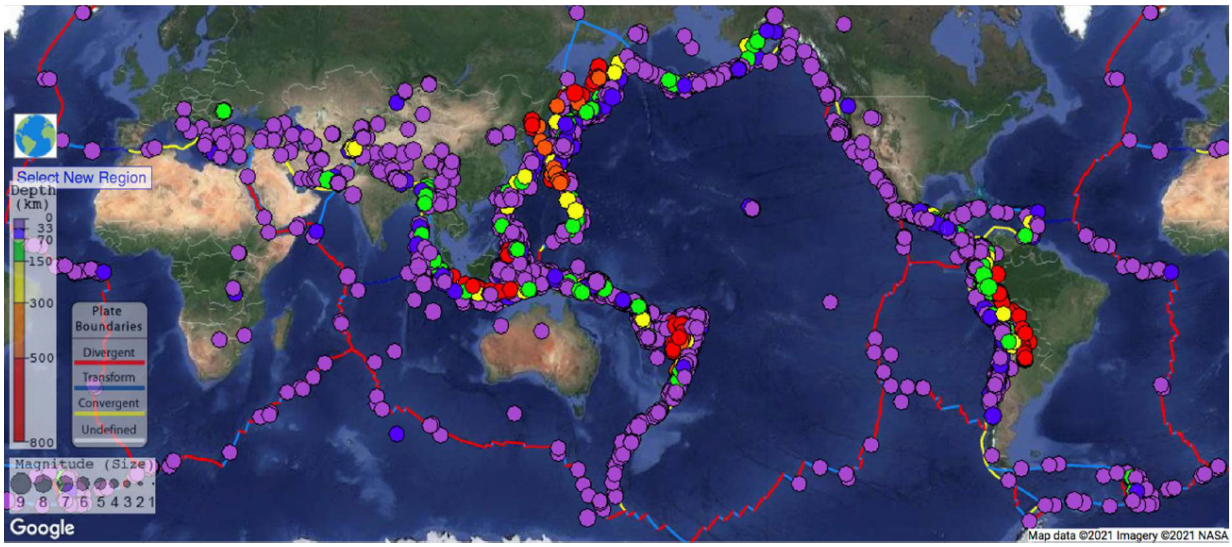

Figure 3: A map of global earthquakes from 1970 to 2020, sampled for 10,000 large events with magnitudes $M_w \geq 6.5$ and varying depths (taken from https://ds.iris.edu/ieb/ accessed at 9/5/21 with a background view using Google/NASA satellite). Notice that the depths are seen as violet circles for 0-33 km below the surface, blue circles for 33-70 km, green circles for 70-150 km, yellow circles for 150-300 km, orange circles for 300-500 km, and red circles for 500-800 km deep.

study. Instead, it is then provided for demonstrating the global earthquake distribution, reflecting potential seismic threats worldwide. It is clear that most of large earthquakes with $M_w \geq 6.5$ occur along the boundary between two colliding plates at depths shallower than 70 km from the surface (violet and blue circles), including the events striking Indonesian territories. Other occurrences of intermediate to deep sources from 70-150 km beneath the surface (green and yellow circles) to a greater depth of more than 300 km (yellow and red circles) are observed in the mainland of South America, mostly at the interface of the Eurasian and Pacific Plates in the East Asian countries, Kuril Islands (Russia), some areas of Indonesia, and regions in the south-west Pacific Ocean far from the Australian east coasts but close to New Zealand.

METHODOLOGY

Global earthquake datasets in this study were downloaded from United States Geological Services (USGS) at https://earthquake.usgs.gov/earthquakes/ and also collected from specific seismic studies listed in Table 1. The datasets included a total of 90 earthquakes occurring worldwide with varying sizes of $4.45 \leq M_w \leq 9.20$ (moderate to strong ground motions) during years of 1960-2015. These are reported in Table 1 in ordered by magnitudes for four different source mechanisms, namely 28 normal-faults, 31 strike-slip faults, 15 reverse faults and 16 subduction-zone earthquakes.

Among the datasets are three strike-slips that ruptured segments of the well-known Sumatran Fault Zone (SFZ) with moderate scales of $M_w \sim 6$ during years of 2007 and 2009 (Salman *et al*., 2020), two relatively large earthquakes of $M_w \sim 7$ - 8 in the subduction-zone off the west coast of Central Sumatra in years of 2007 and 2010 (Ratnasari *et al*., 2020), and a megathrust earthquake of $M_w \sim 9$ popularly known as the 2004 Sumatra-Andaman tectonic release (Fujii & Satake, 2007; Murotani *et al*., 2013) generating the Indian Ocean tsunami that destroyed lives and properties along the west coast of Aceh Province and some north-west regions of Sumatra Island, Indonesia (Suppasri *et al*., 2015).

The inclusion of more than a half of all events (59 cases) classified into normal and strike-slip mechanisms of intermediate sizes guarantees that the results are expected to be relevant to Indonesian settings, as these types of faulting represent frequent occurrences. More active crustal faults have been recently found (Irsyam *et al*., 2017), reflecting future events with possible magnitudes of $M_w \geq 7.5$ (large earthquakes). These points of thought along with megathrust earthquakes possible to occur in the future at the interface between colliding plates with $M_w \sim 9$ are logical reasons why a wide range of earthquake magnitudes induced by the intraplate (strike-slips and dip-slips) and subduction-zone earthquakes were collected for seismic hazard analysis in this study.

RESULTS AND DISCUSSIONS

A list of all the event datasets worldwide considered in the present study can be seen in Table 1, where the corresponding reference study for each event is also given. Notice that information on rupture length L and width W of cases numbered 85-90 is not available but the area A is given.

As early stated, this study has examined all faulting types of events either strike-slip or dip-slip and subduction-zone earthquakes with emphasizing on the $M_w - A$ scaling for each mechanism. This is performed in favor of direct comparisons to the previous results of Thingbaijam *et al*. (2017) except that we do not include other source parameters in scaling relationships, such as the width W and the depth d in this study. In fact, we have worked with the parameters and found relatively unclear patterns of the plot distribution when the M_w scaled with them both. Likewise, we found a less clear relation between M_w and L in the plot distribution relatively compared to the $M_w - A$ scaling. This is because the earthquake size is determined from the seismic moment M_o using a relation $M_w = 0.67 \times (\log M_o - 16.1)$ according to Kanamori (1977; 1983). Whilst, the M_o is related to the fault area A through $M_o = \mu D A$, where μ represents the rigidity and D denotes the average slip (Abe, 1985). It is quite easy to understand that M_w is a logarithmic function of A or equivalently a natural logarithmic function of A. More precisely, we can thus write $M_w \sim \log A$ or $M_w \sim \ln A$ for theoretical scaling.

For this reason, four similarly curved graphs illustrating the empirical scaling of $M_w - A$ relationships for normal, strike-slip, reverse faulting and subduction events are depicted in Figures 4(a), 4(b), 4(c), and 4(d), respectively. As predicted by the theory, the graphs are self-consistent in that they demonstrate dependence of M_w upon A through either a logarithmic proportionality or a natural logarithmic proportionality as is the case in this study, consistent with previous source-scaling laws (Wells & Coppersmith, 1994; Hanks & Bakun, 2002; Shaw, 2009; 2013; Wu *et al*., 2013; Konstantinou, 2014; Goda *et al*., 2016; Thingbaijam *et al*., 2017). The similarity in the $M_w - A$ scaling for all source mechanisms is achieved at greater than 90% confidence (see legends in Figure 4).

An interesting feature shown in Figure 4 is that magnitude M_w grows with respect to rupture area A at slightly different rates for each event type. This is reflected by distinct coefficients of natural logarithmic function for each type of faulting; 0.50 is the largest value for normal faulting in Figure 4(a) down to 0.39, which is the smallest for the plate boundary earthquakes seen in Figure 4(d). The second largest is found to be 0.47 for strike-slips in Figure 4(b), after which 0.40 is observed for reverse faulting in Figure 4(c). The coefficients obtained here are different from the values reported by Thingbaijam *et al*. (2017) in terms of ordered sources from the largest to the smallest. For the normal-faulting events in their study, the coefficient was found to be 0.54, followed by 0.46 for the strike-slips and plate-boundary events, followed by 0.41 for the reverse-faulting at shallow sources (see Table 2).

Table 1: List of global earthquakes datasets with their corresponding source parameters: moment magnitude, rupture length rupture width and rupture area used in this study (ordered by the scale from 4.45 to 9.20 for all event types) from occurrences during 1960-2015 years.

No	Event Date	M_w	L (km)	W (km)	A (km^2)	ln A	Event Type	*References
1	2006/11/17	4.45	2	4	8	2.08	NE	Konstantinou (2014)
2	1996/04/03	5.09	9	4	36	3.58	NE	Konstantinou (2014)
3	1980/02/29	5.16	5	5	25	3.22	NE	Konstantinou (2014)
4	2009/05/24	5.18	6	6	36	3.58	NE	Konstantinou (2014)
5	2010/01/22	5.19	6	5	30	3.40	NE	Konstantinou (2014)
6	2004/02/11	5.29	8	7	56	4.03	NE	Konstantinou (2014)
7	2010/01/18	5.29	6	6	36	3.58	NE	Konstantinou (2014)
8	2009/09/06	5.39	9	6	54	3.99	NE	Konstantinou (2014)
9	1998/09/09	5.43	9	6	54	3.99	NE	Konstantinou (2014)
10	1984/04/29	5.65	14	6	84	4.43	NE	Konstantinou (2014)
11	1997/10/14	5.65	7	4	28	3.33	NE	Konstantinou (2014)
12	1997/09/26	5.67	7	4	28	3.33	NE	Konstantinou (2014)
13	1986/09/13	5.86	10	10	100	4.61	NE	Konstantinou (2014)
14	1997/09/26	5.90	12	5	60	4.09	NE	Konstantinou (2014)
15	1992/10/12	5.95	12	10	120	4.79	NE	Konstantinou (2014)
16	2000/06/06	5.96	13	8	104	4.64	NE	Konstantinou (2014)
17	1999/09/07	6.10	15	17	255	5.54	NE	Konstantinou (2014)
18	1981/03/04	6.23	25	10	250	5.52	NE	Konstantinou (2014)
19	1995/10/01	6.26	24	12	288	5.66	NE	Konstantinou (2014)
20	1995/06/15	6.32	27	11	297	5.69	NE	Konstantinou (2014)
21	2009/04/06	6.32	25	12	300	5.70	NE	Konstantinou (2014)
22	1978/06/20	6.44	28	14	392	5.97	NE	Konstantinou (2014)
23	1981/02/24	6.57	28	17	476	6.17	NE	Konstantinou (2014)
24	1980/07/09	6.59	30	13	390	5.97	NE	Konstantinou (2014)
25	1995/05/13	6.74	28	10	280	5.63	NE	Konstantinou (2014)
26	1980/11/23	6.91	50	14	700	6.55	NE	Konstantinou (2014)
27	1995/11/22	7.21	48	24	1152	7.05	NE	Konstantinou (2014)
28	2001/01/13	7.70	101	39	3939	8.28	NE	Tanioka *et al.* (2017)
29	2005/09/08	4.47	2.5	2	5	1.61	SSE	Konstantinou (2014)
30	1996/07/15	4.76	2.5	4	10	2.30	SSE	Konstantinou (2014)
31	1996/02/18	5.12	5	7	35	3.56	SSE	Konstantinou (2014)
32	2012/01/27	5.38	8	6	48	3.87	SSE	Konstantinou (2014)
33	1996/10/15	5.39	9	5	45	3.81	SSE	Konstantinou (2014)
34	2002/12/02	5.48	5	6	30	3.40	SSE	Konstantinou (2014)
35	2002/11/01	5.66	8	8	64	4.16	SSE	Konstantinou (2014)
36	2003/07/06	5.68	10	6	60	4.09	SSE	Konstantinou (2014)
37	1998/04/12	5.73	13	7	91	4.51	SSE	Konstantinou (2014)
38	1985/10/27	5.77	14	10	140	4.94	SSE	Konstantinou (2014)
39	2002/10/31	5.79	6	13	78	4.36	SSE	Konstantinou (2014)
40	2013/01/08	5.83	10	8	80	4.38	SSE	Konstantinou (2014)
41	1994/05/26	5.86	16	8	128	4.85	SSE	Konstantinou (2014)
42	2003/08/14	6.08	25	10	250	5.52	SSE	Konstantinou (2014)
43	1999/10/22	6.12	13.9	13.8	191	5.25	SSE	Yen & Ma (2011)
44	2007/03/06	6.30	22	9	198	5.29	SSE	Salman *et al.* (2020)
45	1994/06/05	6.31	8.9	8.3	73	4.30	SSE	Yen & Ma (2011)
46	1998/06/27	6.33	30	18	540	6.29	SSE	Konstantinou (2014)

No	Event Date	M_w	L (km)	W (km)	A (km^2)	ln A	Event Type	*References
47	2004/02/24	6.35	19	12	228	5.43	SSE	Konstantinou (2014)
48	2007/03/07	6.40	25	10	250	5.52	SSE	Salman *et al*. (2020)
49	2008/06/08	6.40	30	10	300	5.70	SSE	Konstantinou (2014)
50	2001/07/26	6.45	27	14	378	5.93	SSE	Konstantinou (2014)
51	2009/10/01	6.60	33	11	363	5.89	SSE	Salman *et al*. (2020)
52	1992/03/13	6.66	30	10	300	5.70	SSE	Konstantinou (2014)
53	2006/12/26	6.80	29.8	24.3	725	6.59	SSE	Yen & Ma (2011)
54	1995/01/17	6.90	57	18	1027	6.93	SSE	Murotani *et al*. (2015)
55	1999/11/12	7.11	55	17	935	6.84	SSE	Konstantinou (2014)
56	1992/06/28	7.20	74	14.7	1090	6.99	SSE	Murotani *et al*. (2015)
57	1999/08/17	7.50	126	19.8	2499	7.82	SSE	Murotani *et al*. (2015)
58	2001/11/14	7.76	319	28.5	9078	9.11	SSE	Yen & Ma (2011)
59	2002/11/03	7.90	320	24.5	7827	8.97	SSE	Murotani *et al*. (2015)
60	1998/07/17	5.88	8.1	5.4	44	3.79	RE	Yen & Ma (2011)
61	1989/10/29	5.90	13	10	130	4.87	RE	Konstantinou (2014)
62	2003/06/9	5.92	6.7	7.1	48	3.87	RE	Yen & Ma (2011)
63	1979/05/24	6.20	17	11	187	5.23	RE	Konstantinou (2014)
64	1999/09/22	6.23	17.3	16.3	282	5.64	RE	Yen & Ma (2011)
65	1999/09/25	6.35	16.3	15.1	245	5.50	RE	Yen & Ma (2011)
66	1976/05/06	6.51	25	15	375	5.93	RE	Konstantinou (2014)
67	2003/05/21	6.94	50	15	750	6.62	RE	Konstantinou (2014)
68	1979/04/15	7.06	50	23	1150	7.05	RE	Konstantinou (2014)
69	1978/09/16	7.09	74	30.1	2227	7.71	RE	Yen & Ma (2011)
70	2001/01/26	7.38	31.6	25.2	798	6.68	RE	Yen & Ma (2011)
71	2005/10/08	7.50	120	36	4320	8.37	RE	Murotani *et al*. (2015)
72	1999/09/20	7.60	89	38.6	3435	8.14	RE	Murotani *et al*. (2015)
73	1985/09/19	8.01	158.6	115	18245	9.81	RE	Yen & Ma (2011)
74	2008/05/12	8.01	243.7	30.6	7462	8.92	RE	Yen & Ma (2011)
75	2004/10/09	7.00	36	22	792	6.67	SE	Tanioka *et al.* (2017)
76	2012/08/27	7.30	50	28	1400	7.24	SE	Tanioka *et al.* (2017)
77	1992/09/02	7.60	100	52	5200	8.56	SE	Tanioka *et al.* (2017)
78	2010/10/25	7.80	103	51	5253	8.57	SE	Ratnasari *et al*. (2020)
79	2013/02/06	8.00	60	140	8400	9.04	SE	Heidarzadeh *et al*. (2016)
80	2007/01/13	8.10	290	90	26100	10.17	SE	Lobkovsky *et al*. (2009)
81	2014/04/01	8.10	157.5	105	16538	9.71	SE	Lay *et al*. (2014)
82	2006/11/15	8.30	300	220	66000	11.10	SE	Lobkovsky *et al*. (2009)
83	2015/09/16	8.30	230	100	23000	10.04	SE	Ren *et al*. (2017)
84	2007/09/12	8.40	208	91	18928	9.85	SE	Ratnasari *et al*. (2020)
85	2005/03/28	8.60	-	-	40000	10.60	SE	Walker *et al*. (2005)
86	2010/02/27	8.80	-	-	62500	11.04	SE	Murotani *et al*. (2013)
87	2011/03/11	9.00	-	-	92500	11.43	SE	Murotani *et al*. (2013)
88	1964/03/27	9.10	-	-	164160	12.01	SE	Murotani *et al*. (2013)
89	2004/12/26	9.10	-	-	160000	11.98	SE	Murotani *et al*. (2013)
90	1960/05/22	9.20	-	-	135000	11.81	SE	Murotani *et al*. (2013)

NE = Normal Event, SSE = Strike-Slip Event, RE = Reverse Event, SE = Subduction Event
Cases 1-28: Normal faulting earthquakes with magnitudes ranging from 4.45 to 7.70
Cases 29-59: Strike-slip faulting earthquakes with magnitudes ranging from 4.47 to 7.90
Cases 60-74: Reverse faulting earthquakes with magnitudes ranging from 5.88 to 8.01
Cases 75-90: Subduction-zone earthquakes with magnitudes ranging from 7.00 to 9.20
*References refer to the source parameters of the events determined by the published studies.

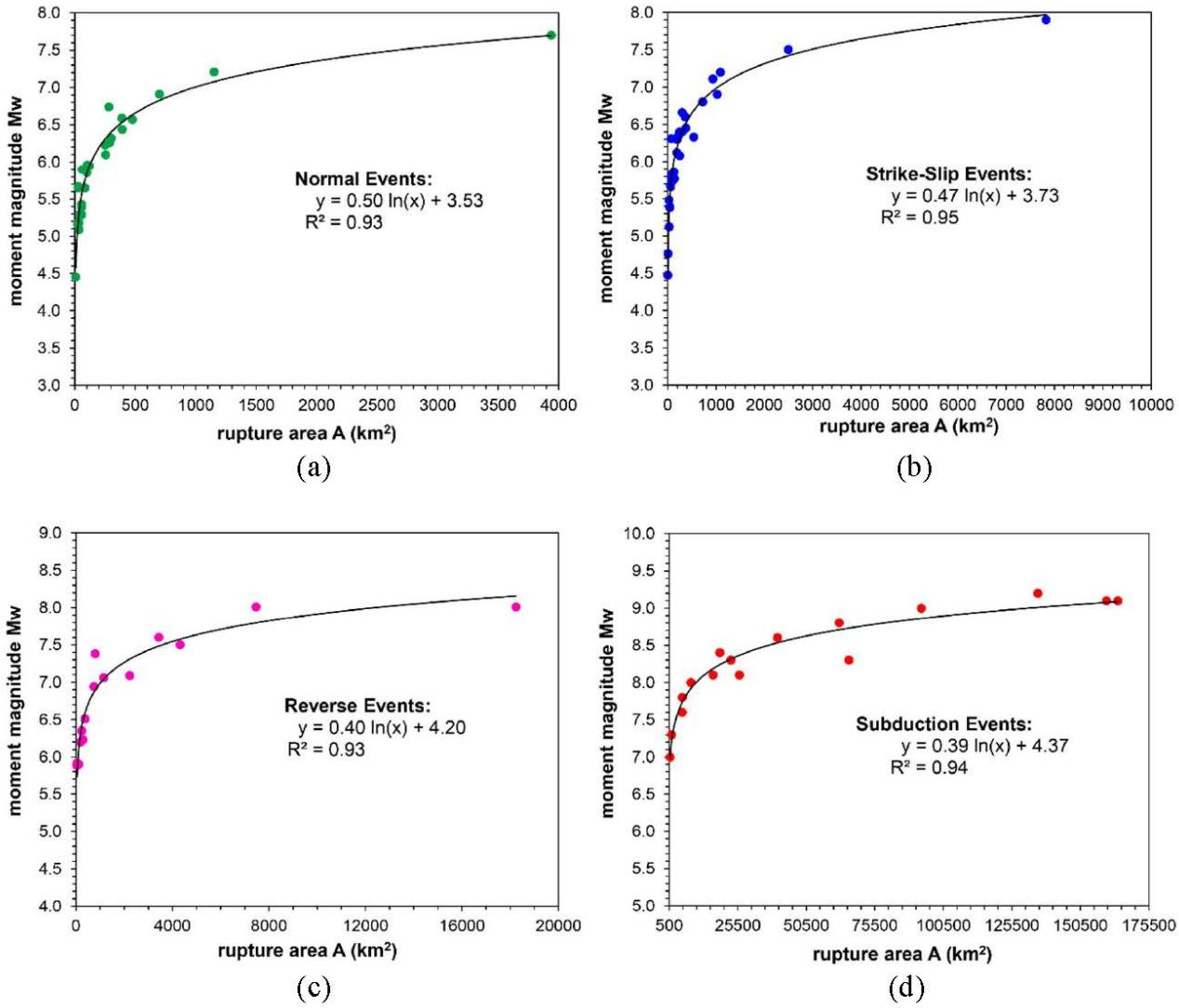

Figure 4: Four graphs showing moment magnitude-rupture area $M_w - A$ scaling relationship for cases of (a) normal faulting with 28 events in green, (b) strike-slip faulting with 31 events in blue, (c) reverse faulting with 15 events in pink, and (d) subduction-zone earthquakes with 16 events in red; all events are extracted from the datasets for each type of source mechanism reported in Table 1.

One of logical reasons why a discrepancy in the logarithmic coefficients between our study and Thingbaijam *et al.* (2017) appears is that they utilised orthogonal regressions instead of least-squares regressions, as is the case in this study. Another logical reason may actually be from the difference in global earthquake datasets between the ones currently used in this study and those in Thingbaijam *et al.* (2017).

Unfortunately, the present results cannot be directly compared to those of Goda *et al.* (2016) as they divided the $M_w - A$ scaling into cases of tsunamigenic and non-tsunamigenic, irrelevant to this work. However, apart from this irrelevance and the disordered mechanisms (compared to the reference of Thingbaijam *et al.* (2017) in terms of coefficients for natural logarithmic function), this study yields good estimates in earthquake size of past events.

The followings are good examples of how close magnitude estimates by the scaling relations developed from this study, relatively compared to reference values. The first case to consider is a moderate event that occurred near Fukushima Prefecture in the east coast of Japan on November 21, 2016 at 20:59:47 Universal Time Coordinates (UTC). The event was caused by ground motions of a normal fault sized of M_w 6.9 by USGS. Taking the fault area of 39 × 17 km^2 given by the model of Suppasri *et al.* (2017), we use $M_w = 0.50 \ln A + 3.53$ in Figure 4(a) for this event to obtain $M_w = 6.78$, less than 2% different from that reported by USGS and consistent with that predicted by Thingbaijam *et al.* (2017). The second case to discuss is that the shocking event on September 28, 2018 at about 10:02:44 UTC, after which

it was widely known as the 2018 Palu-Donggala strike-slip earthquake sized of M_w7.5 recorded by USGS, inducing a relatively large tsunami inside Palu Bay (Supendi *et al*., 2020). Taking fault area of 200 × 15 km^2 in Gusman *et al*. (2019), we here apply $M_w = 0.47 \ln A + 3.73$ as seen in Figure 4(b) to obtain $M_w = 7.49$, which is almost the same as that reported by USGS and again consistent with that predicted by Thingbaijam *et al*. (2017).

A further example is given for a reverse (thrust) faulting slip that occurred in Nepal, close to a collision zone of Indian Plate and Tibetan Plateau of relatively high seismicity on April 25, 2015 at 06:11:25 with M_w 7.8 (USGS). The energy release mechanism was similar to ones in the subduction interface, where the Himalayan Thrust Fault slipped over the Indian Plate (Kumar *et al*., 2017). Using a rupture model for the thrust event of a 150 km long and 70 km wide plane (Kumar *et al*., 2017) and the relevant scaling $M_w = 0.40 \ln A + 4.20$ from Figure 4(c), we have $M_w = 7.90$, which is only 1% deviation, insignificant different from that recorded by USGS.

To complete examples of faulting events both from strike-slip and dip-slip which were well predicted by relevant empirical scaling developed from this study, we here provide two cases of subduction-zone earthquakes. The first case to discuss is that a relatively strong ground motion striking Chiloé Island in Chilean southern district was recorded as M_w 7.5 by USGS on December 25, 2016 at 14:22:27 UTC. The fault model developed by Xu (2017) suggested a thrust-fault motion, triggering a tectonic release of about M_w7.6 by which the same segment was ruptured in the 1960 Chilean megathrust of M_w 9.2 (Fujii & Satake, 2012; Murotani *et al*., 2013), the largest event recorded in the history. Using the model of 48 km in length × 76 km in width (Xu, 2017) and the scaling $M_w = 0.39 \ln A + 4.37$ from Figure 4(d), we estimate $M_w = 7.57$. Then, the size difference between the value provided by the scaling and the reference given by USGS is 1%, considered unimportant.

Although the four recent large events fill examples having insignificant differences in earthquake magnitude estimates between predicted values using the empirical scaling laws used in this study and the ones given by the USGS, all the cases provided are lack of an event with M_w 8.0 that is considered as a megathrust subduction earthquake in the plate boundary. This event is potential to generate a large tsunami wave following the quake. Tsunamis, along with causative ocean floor deformation from major events, are of practical interest for tsunami-seismic assessment and analysis as the catastrophes may be present simultaneously. For instance, strong ground-motions found in the Kuril Islands, Russia on November 15, 2006 with M_w 8.3 and two months later on January 13, 2007 with M_w 8.1 generated strong tsunamis with relatively large waves striking most regions in the whole Pacific (Lobkovsky *et al*., 2009). This previous study is interesting in that the scenarios for the two devastating seismic and corresponding tsunami hazards in the source region were predicted earlier. Accurate prediction involved the concept of a seismic gap for a megathrust earthquake and its associated destructive tsunami wave possible to occur in the region of interest at any time as long as some seismic conditions were fulfilled.

A seismic gap hypothesis (McCann *et al*., 1979; Nishenko, 1991; Rong *et al*., 2003; Lobkovsky *et al*., 2009) points out the most possible region, as part of a larger area with high seismicity, where ground motions with strong sizes due to considerable amounts of crustal deformation have long been absent. This particular region is predicted to undergo a future catastrophic seismic event with a high probability. Within this context, Widiyantoro *et al*. (2020) reported the gaps close to Java Trench (see Figure 1) off the south coast of Java Island based on three seismic scenarios. The scenarios included the worst case where the double (see western and eastern Java segments in Figure 2) megathrust segments ruptured at the same time. If it occurs, megathrust earthquakes with corresponding large tsunami waves are likely to produce with a height of ~ 5 m on average along the southern coastal lines of Java Island but possibly reaching as high as ~ 20 m and ~ 12 m in particular regions of West Java and East Java, respectively (Widiyantoro *et al*., 2020).

Interestingly, the three scenarios described by Widiyantoro *et al*. (2020) correspond to separate megathrust seismic energy releases, measured by event magnitudes of M_w 8.9 when the western Java segment collapses, M_w 8.8 when the eastern Java segment collapses, and M_w 9.1 when both segments rupture simultaneously (see Figure 2). Here, we intend to test these possible catastrophes by applying our finding on the empirical scaling relation for the megathrust subduction-zone earthquakes. We use $M_w = 0.39 \ln A + 4.37$ provided in Figure 4(d) and a modeled faulting-plane of 660 km long and 210 km wide (Widiyantoro *et al*., 2020) to obtain $M_w = 8.99$. This result is remarkable in the sense that it is slightly different, by ~ 2% only, from the sizes calculated by Widiyantoro *et al*. (2020).

Our source-scaling estimate is supported by a numerical work of Corbi *et al*. (2019) using their scaling of $M_w = 0.37 \log A + 4.44$ (equivalent to $M_w = 0.441 \log A + 8.446$ in its original form of the work) for datasets of subduction earthquakes of sizes $6.2 \leq M_w \leq 8.3$. Applying the scaling of Corbi *et al*. (2019) with the fault-plane geometry of 138,600 km^2 by Widiyantoro *et al*. (2020), we then have $M_w = 8.82$, slightly different from that based on our scaling estimate.

Having tested the scaling in this study successfully, we compare them all with those of Thingbaijam *et al*. (2017) given in Table 2. The largest rupture area for each event type (see Table 1) is substituted into the equivalent source-scaling relationships of Thingbaijam *et al*. (2017) and the ones in this study. The difference in size between calculated magnitudes in percentage is seen in the last column of Table 2 (magnitudes given by previous work are references).

It is clear from Table 2 that predicted magnitudes of lithospheric motions either by strike-slip or dip-slip intraplate

Table 2: Comparisons between source-scaling relations of Thingbaijam *et al*. (2017) with the corresponding relations found from this study for all source event mechanisms, independent of the depth, showing a linier-natural log of the $M_w - A$ scaling.

No	Source Mechanism	Thingbaijam *et al*. (2017)	This Study	*Diff. in size estimate (%)
1	Normal Faulting	$M_w = 0.54 \ln A + 3.16$	$M_w = 0.50 \ln A + 3.53$	0.5
2	Strike-Slip Faulting	$M_w = 0.46 \ln A + 3.70$	$M_w = 0.47 \ln A + 3.73$	1.5
3	Reverse Faulting	$M_w = 0.41 \ln A + 4.16$	$M_w = 0.40 \ln A + 4.20$	0.7
4	Subduction Processes	$M_w = 0.46 \ln A + 3.47$	$M_w = 0.39 \ln A + 4.37$	0.7

*Diff. in size estimate = the fractional difference in M_w calculated using the empirical scaling derived from this study and that of Thingbaijam *et al*. (2017).

faulting and by subduction-zone processes using the source-scaling relations in this study are in good agreement with the values calculated by the scaling laws reported by Thingbaijam *et al*. (2017) to within ± 0.1. The only small difference of less than 2% in the earthquake size estimates between this study and Thingbaijam *et al*. (2017) provides a notable progress with respect to the previous source-scaling laws (Wells & Coppersmith, 1994; Hanks & Bakun, 2002; Shaw, 2009; Konstantinou, 2014). Indeed, the current results are well suited for tsunami-seismic hazard analysis and its corresponding disaster risk assessment.

Although Goda *et al*. (2016) suggested separate $M_w - A$ scaling for tsunamigenic and non-tsunamigenic occurrences, these are limited in applications. Large tsunamis generated by both strike-slip and normal-faulting slip are rare but possible to occur. Cases of the 2016 Kaikoura, New Zealand (Power *et al*., 2017) and the 2018 Palu Bay, Indonesia (e.g., Gusman *et al*., 2019) were exceptional to list, where strike-slip fault movement induced destructive tsunamis. Hence, the separate $M_w - A$ scaling relations for each type of source mechanism are of favorable significance for possible use worldwide in the future.

To further characterise seismic records of strong-motions from faulting-slips and the plate boundary, we analyse functional relationships of $M_w - A$ scaling obtained from this study for all the four sources in one plot, depicted in Figure 5. Except for the earthquakes at the plate interface, depicted as the red solid-curve, the other three types of events are given in dashed-curves using hypothetical faulting-plane data from 4×10^4 km^2 to a point before reaching the maximum earthquake magnitude measured ever in the history of seismic hazards worldwide, the 1960 Chilean event (Fujii & Satake, 2012; Murotani *et al*., 2013).

The empirical scaling relations derived from this study can also be used to assess tsunami hazard generated by future giant earthquakes possible. The rupture area A can be estimated based upon the scaling relations if the earthquake size observed in M_w is known. Conversely, an earthquake size of any faulting type and source mechanism can then possibly be estimated accurately from a modeled source area.

It is clear from Figure 5 that the size of normal earthquakes varies rapidly with the area in particular for a limited range from ~ 10^3 to ~ 3×10^4 km^2. In this range, a relatively small increase in the area will correspond to a considerable amount of change in the event size. Further, a similar situation is also found for other sources (strike-slip and reverse faulting). However, the area never reaches a definite value in which the maximum magnitude M_w= 9.3 (the black dashed-line) would be possible to achieve.

In the case of subduction earthquakes, the magnitude grows slowly at a low rate with respect to the area. The size scales with M_w ~ 9.0 at $A \approx 1.6 \times 10^5$ km^2, after which it seems to achieve an asymptote at a value that is close to an upper bound on the magnitude observed ever

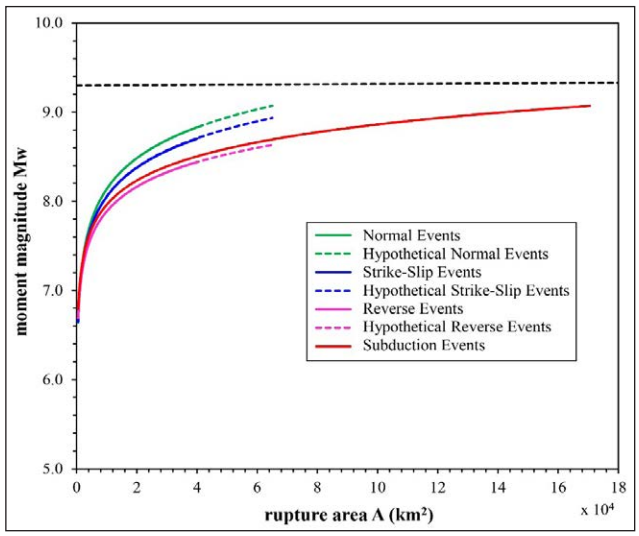

Figure 5: Modified graphs showing the four $M_w - A$ scaling relationships for (a) normal (green), (b) strike-slip (blue), (c) reverse (pink), and (d) subduction-zone (red) earthquakes from the datasets in Table 1. The green, blue, and pink curved solid-lines are created by hypothetical data with the rupture area of 0 to 4×10^4 km^2 while the continuing curved dashed-lines in green, blue, and pink represent the hypothetical data of each corresponding colour. The black horizontal dashed-line shows a line of $M_w \approx 9.3$ that would likely serve as the maximum magnitude possible, close to the observed magnitude M_w 9.2 for the great 1960 Chilean event (Fujii & Satake, 2012; Murotani *et al*., 2013).

M_w= 9.2 in the 1960 Chilean event (Fujii & Satake, 2012; Murotani *et al*., 2013) at very large faulting dimensions. Within this context, we double the largest area (see Table 1), equivalent to A ≈ 3.2 × 10^5 km^2 for the maximum fault area of the subduction earthquakes in Thingbaijam *et al*. (2017) to account for the very large area possible. Inserting this value into a scaling developed by Goda *et al*. (2016) for tsunamigenic events M_w= 0.55 ln *A* + 2.24 results in M_w= 9.21. When we substitute the same area into equivalently-empirical scaling of Thingbaijam *et al*. (2017) for calculation of energy release in the subduction interface (see Table 2), we obtain M_w= 9.30. For comparison, using M_w= 0.39 ln *A* + 4.37 in the same table from the present study, we have M_w= 9.31. All of these estimates, based on distinct considerations, are hence similar numbers to within ± 0.1, acceptable for errors in magnitude measurements in most seismic studies. This suggests that predicted magnitudes of M_w ~ 9.0 following a future megathrust subduction-zone earthquake due to the scenarios proposed by Widiyantoro *et al.* (2020) is thus possible to occur.

CONCLUSIONS

A study on earthquake size prediction has been performed by deriving empirical scaling relationships of the rupture area *A* and corresponding moment magnitude M_w. Using a total of 90 events from the global datasets of sizes 4.45 ≤ M_w ≤ 9.20 during years of 1960-2015, we have examined normal, strike-slip, reverse and subduction-zone events, and found M_w= 0.50 ln *A* + 3.53, M_w= 0.47 ln *A* + 3.73, M_w= 0.40 ln *A* + 4.20 and M_w= 0.39 ln *A* + 4.37, respectively for each type of source mechanism. The results suggest that the size scale for subduction-zone events asymptotes to a value of M_w ≈ 9.3 possible to reach at rupture areas much larger than those for the strike-slips and dip-slips. It follows that seismic energy release following tectonic activities at the interplate-boundary is potential to generate megathrust earthquakes. Hence, these are relevant to Indonesian geological and tectonic settings, where the subduction-zone earthquake is considered to be a persistent seismic threat for the nation apart from the more active continental faults being recently found in most of Indonesian territories. In particular, a future event with magnitude of M_w ~ 9.0 remains possible to occur off the south coastal regions of Java Island, having the largest population in Indonesia. This key result confirms the magnitudes predicted by seismic collapses of the two Java segments (Widiyantoro *et al.*, 2020). Therefore, the current results suggest better disaster preparedness and increasing awareness of significance of an integrated tsunami-earthquake early warning with a high priority for early detection of potential seismic threats, particularly in the most vulnerable regions in Indonesia to all future possible tsunami-seismic hazards.

ACKNOWLEDGEMENTS

The authors would greatly like to thank United States Geological Survey (USGS) from which the global earthquake datasets used are available at https://earthquake.usgs.gov/earthquakes/ and those with their published studies listed in Table 1. The authors would also like to thank Incorporated Research Institutions for Seismology (IRIS) for providing IRIS Earthquake Browser (IEB) at https://ds.iris.edu/ieb/, with which a map of global earthquakes is produced. As well, great thanks go to ArcGIS Online Basemaps at https://arcgis.com/home/group.html, with which high-resolution maps of the world imagery and Indonesian territories are made. The work has also benefited constructive comments and suggestions from the GSM Editor and two anonymous reviewers during a fairly reviewing process.

AUTHOR CONTRIBUTIONS

TP initially introduces a research topic to the members of the research group and writes a draft with some necessary changes over time through the development of the research. He is responsible for data collection and analysis, and interpretation of the results. He provides the final approval of the work both before a submission and within a reviewing process, during which substantial changes are made by taking into account all comments and suggestions by the GSM Editor and two anonymous reviewers.

GPA gives her best to discuss the topic with the other members of the group, reads carefully the draft and its continual changes during the progress of the research. She joins TP to collect datasets from the USGS site and published studies. She also critically reviews research sources available, helps analyse the datasets and interprets the associated results, and helps prepare for the revised manuscript for a final inspection by TP.

HR follows discussions on the topic with the group members, provides the second opinion, and reads carefully the draft and its changes after discussions. In particular, she creates the majority of the figures in the manuscript required for visualising the texts in paragraphs throughout the work. She also helps prepare for the revised work for a final inspection by TP.

CONFLICT OF INTEREST

The authors declare that there is no conflict of interest regarding this work.

REFERENCES

Abe, K., 1985. Quantification of major earthquake tsunamis of the Japan Sea. Physics of the Earth and Planetary Interiors, 38(4), 214-223, doi: 10.1016/0031-9201(85)90069-X.

Cipta, A., Robiana, R., Griffin, J.D., Horspool, N., Hidayati, S. & Cummins, P., 2016. A probabilistic seismic hazard assessment for Sulawesi, Indonesia. In: Cummins, P.R. & Meilano, I. (Eds.), Geohazards in Indonesia: Earth Science for Disaster Risk Reduction. Geological Society of London: Special

Publications, 441(1), doi: 10.1144/SP441.6.

Corbi, F., Sandri, L., Bedford, J., Funiciello, F., Brizzi, S., Rosenau, M. & Lallemand, S., 2019. Machine learning can predict the timing and size of analog earthquakes. Geophysical Research Letters, 46(3), 1303-1311, doi: 10.1029/2018GL081251.

Cummins, P.R., 2017. Geohazards in Indonesia: Earth science for disaster risk reduction–introduction. Geological Society of London: Special Publications, 441, 1-7, doi: 10.1144/SP441.11.

Fujii, Y. & Satake, K., 2007. Tsunami source of the 2004 Sumatra-Andaman earthquake inferred from tide gauge and satellite data. Bulletin of the Seismological Society of America, 97, S192-S207, doi: 10.1785/0120050613.

Fujii, Y. & Satake, K., 2012. Slip distribution and seismic moment of the 2010 and 1960 Chilean earthquakes inferred from tsunami waveforms and coastal geodetic data. Pure and Applied Geophysics, 170(9), 1493-1509, doi: 10.1007/s00024-012-0524-2.

Goda, K., Yasuda, T., Mori, N. & Maruyama, T., 2016. New scaling relationships of earthquake source parameters for stochastic tsunami simulation. Coastal Engineering Journal, 58(3), 1650010(1-40), doi: 10.1142/S0578563416500108.

Gunawan, E. & Widiyantoro, S., 2019. Active tectonic deformation in Java, Indonesia inferred from a GPS-derived strain rate. Journal of Geodynamics, 123, 49-54, doi: 10.1016/j.jog.2019.01.004.

Gusman, A.R., Supendi, P., Nugraha, A.D., Power, W., Latief, H., Sunendar, H., Widiyantoro, S., Daryono., Wiyono, S. H., Hakim, A., Muhari, A., Wang, X., Burbidge, D., Palgunadi, K., Hamling, I. & Daryono, M. R., 2019. Source model for the tsunami inside Palu Bay following the 2018 Palu earthquake, Indonesia. Geophysical Research Letters, 46(15), 8721-8730, doi: 10.1029/2019GL082717.

Hanks, T.C. & Bakun, W.H., 2002. A bilinear source-scaling model for M-log A observations of continental earthquakes. Bulletin of the Seismological Society of America, 92(5), 1841-1846, doi: 10.1785/0120010148.

Heidarzadeh, M., Harada, T., Satake, K., Ishibe, T. & Gusman, A.R., 2016. Comparative study of two tsunamigenic earthquakes in the Solomon Islands: 2015 Mw 7.0 normal-fault and 2013 Santa Cruz Mw 8.0 megathrust earthquakes. Geophysical Research Letters, 43, 4340-4349, doi: 10.1002/2016GL068601.

Indonesian Bureau of Statistics, 2020. The results of Indonesian population census and density (translation in English). Berita Resmi Statistik No. 7/01/Th. XXIV, Kementerian Dalam Negeri RI (in Indonesian language), 1-12.

Irikura, K., Miyakoshi, K., Kamae, K., Yoshida, K., Somei, K., Kurahashi, S. & Miyake, H., 2017. Applicability of source scaling relations for crustal earthquakes to estimation of the ground motions of the 2016 Kumamoto earthquake. Earth, Planets, and Space, 69(10), doi: 10.1186/s40623-016-0586-y.

Irsyam, M.I., Widiyantoro, S., Natawidjaja, D.H., Meilano, I., Rudiyanto, A., Hidayati, S., Triyoso, W., Hanifa, N.R., Djarwadi, D. & Faizal, L., 2017. Source Map of the 2017 Indonesian Earthquake Hazard (translation in English). 1st Ed. Penerbit Pusat Studi Gempa Nasional (PUSGEN) dan Pusat Litbang Perumahan dan Permukiman, Kementerian Pekerjaan Umum dan Perumahan Rakyat (PUPR) (in Indonesian language), ISBN: 978-602-5489-01-3, Bandung, Indonesia. 1-400.

Kanamori, H., 1977. The energy release in great earthquakes. Journal of Geophysical Research, 82(20), 2981-2987, doi: 10.1029/JB082i020p02981.

Kanamori, H., 1983. Magnitude scale and quantification of earthquakes. Tectonophysics, 93(3-4), 185-199, doi: 10.1016/0040-1951(83)90273-1.

Konstantinou, K.I., 2014. Moment magnitude-rupture area scaling and stress-drop variations for earthquakes in the Mediterranean region. Bulletin of the Seismological Society of America, 104(5), 2378-2386, doi: 10.1785/0120140062.

Koulali, A., Susilo, S., McClusky, S., Meilano, I., Cummins, P., Tregoning, P., Lister, G., Efendi, J. & Syafi'I, M.A., 2016. Crustal strain partitioning and the associated earthquake hazard in the eastern Sunda-Banda Arc. Geophysical Research Letters, 43(5), 1943-1949, doi: 10.1002/2016GL067941.

Koulali, A., McClusky S., Susilo, S., Leonard, Y., Cummins, P., Tregoning P., Meilano, I., Efendi, J. & Wijanarto, A.B., 2017. The kinematics of crustal deformation in Java from GPS observations: implications for fault slip partitioning. Earth and Planetary Science Letters, 458, 69-79, doi: 10.1016/j.epsl.2016.10.039.

Kumar, A., Singh, S.K., Mitra, S., Priestley, K.F. & Dayal, S., 2017. The 2015 April 25 Gorkha (Nepal) earthquake and its aftershocks: implications for lateral heterogeneity on the Main Himalayan Thrust. Geophysical Journal International, 208(2), 992-1008, doi: 10.1093/gji/ggw438.

Lange, D., Tilmann, F., Henstock, T., Rietbrock, A., Natawidjaja, D. & Kopp, H., 2018. Structure of the central Sumatran subduction zone revealed by local earthquake travel-time tomography using an amphibious network. Solid Earth, 9(4), 1035-1049, doi: 10.5194/se-9-1035-2018.

Lay, T., Yue, H., Brodsky, E.E. & An, C., 2014. The 1 April 2014 Iquique, Chile, Mw 8.1 earthquake rupture sequence. Geophysical Research Letters, 41, 3818-3825, doi: 10.1002/2014GL060238.

Lobkovsky, L.I., Rabinovich, A.B., Kulikov, E.A., Ivashchenko, A.I., Fine, I.V., Thomson, R.E., Ivelskaya, T.N. & Bogdanov, G.S., 2009. The Kuril earthquakes and tsunamis of November 15, 2006, and January 13, 2007: observations, analysis, and numerical modeling. Oceanology, 49(2), 166-181, doi: 10.1134/S0001437009020027.

Marzocchi, W., Sandri, L., Heuret, A. & Funiciello, F., 2016. Where giant earthquakes may come. Journal of Geophysical Research: Solid Earth, 121(10), 7322-7336, doi: 10.1002/2016JB013054.

McCann, W.R., Nishenko, S.P., Sykes, L.R. & Krause, J., 1979. Seismic gaps and plate tectonics: Seismic potential for major boundaries. Pure and Applied Geophysics, 117(6), 1082-1147, doi: 10.1007/978-3-0348-6430-5_2.

Murotani, S., Satake, K. & Fujii, Y., 2013. Scaling relations of seismic moment, rupture area, average slip, and asperity size for $M_w \sim 9$ subduction-zone earthquakes. Geophysical Research Letters, 40(19), 5070-5074, doi: 10.1002/grl.50976.

Murotani, S., Matsushima, S., Azuma, T., Irikura, K. & Kitagawa, S., 2015. Scaling relations of source parameters of earthquakes occurring on inland crustal mega-fault systems. Pure and Applied Geophysics, 172(5), 1371-1381, doi: 10.1007/s00024-014-1010-9.

Nishenko, S.P., 1991. Circum-Pacific seismic potential 1989-1999. Pure and Applied Geophysics, 135(2), 169-259, doi: 10.1007/BF00880240.

Power, W., Clark, K., King, D.N., Borrero, J., Howarth, J. & Lane, E.M., 2017. Tsunami runup and tide-gauge observations from

the 14 November 2016 M 7.8 Kaikoura earthquake, New Zealand. Pure and Applied Geophysics, 174(7), 2457-2473, doi: 10.1007/s00024-017-1566-2.

Ratnasari, R.N., Tanioka, Y. & Gusman, A.R., 2020. Determination of source models appropriate for tsunami forecasting: application to tsunami earthquakes in central Sumatra, Indonesia. Pure and Applied Geophysics, 177(6), 2551-2562, doi: 10.1007/s00024-020-02483-3.

Ren, Z., Yuan, Y., Wang, P., Fan, T., Wang, J. & Hou, J. 2017. The September 16, 2015 Mw 8.3 Illapel, Chile earthquake: Characteristics of tsunami wave from near-field to far-field. Acta Oceanologica Sinica, 36(5), 73-82, doi: 10.1007/s13131-017-1005-3.

Rong, Y., Jackson, D.D. & Kagan, Y.Y., 2003. Seismic gaps and earthquakes. Journal of Geophysical Research, 108(B10), 2471, doi: 10.1029/2002JB002334.

Salman, R., Lindsey, E.O., Feng, L., Bradley, K., Wei, S., Wang, T., Daryono, M.R. & Hill, E.M., 2020. Structural controls on rupture extent of recent Sumatran Fault Zone earthquakes, Indonesia. Journal of Geophysical Research: Solid Earth, 125(2), 1-19, doi: 10.1029/2019JB018101.

Satriano, C., Wu, Y.M., Zollo, A. & Kanamori, H., 2011. Earthquake early warning: concepts, methods, and physical grounds. Soil Dynamics and Earthquake Engineering, 31(2), 106-118, doi: 10.1016/j.soildyn.2010.07.007.

Shaw, B.E., 2009. Constant stress drop from small to great earthquakes in magnitude-area scaling. Bulletin of the Seismological Society of America, 99(2A), 871-875, doi: 10.1785/0120080006.

Shaw, B.E., 2013. Earthquake surface slip-length data is fit by constant stress drop and is useful for seismic hazard analysis. Bulletin of the Seismological Society of America, 103(2A), 876-893, doi: 10.1785/0120110258.

Supendi, P., Nugraha, A.D., Widiyantoro, S., Pesicek, J.D., Thurber, C.H., Abdullah, C.I., Daryono, D., Wiyono, S.H., Shiddiqi, H.A. & Rosalia, S., 2020. Relocated aftershocks and background seismicity in eastern Indonesia shed light on the 2018 Lombok and Palu earthquake sequences. Geophysical Journal International, 221, 1845-1855, doi: 10.1093/gji/ggaa118.

Suppasri, A., Goto, K., Muhari, A., Ranasinghe, P., Riyaz, M., Affan, M., Mas, E., Yasuda, M. & Imamura, F., 2015. A decade after the 2004 Indian Ocean Tsunami: the progress in disaster preparedness and future challenges in Indonesia, Sri Lanka, Thailand and Maldives. Pure and Applied Geophysics, 172(12), 3313-3341, doi: 10.1007/s00024-015-1134-6.

Suppasri, A., Leelawat, N., Latcharote, P., Roeber, V., Yamashita, K., Hayashi, A., Ohira, H., Fukui, K., Hisamatsu, A., Nguyen, D. & Imamura, F., 2017. The 2016 Fukushima earthquake and tsunami: local tsunami behavior and recommendations for tsunami disaster risk reduction. International Journal of Disaster Risk Reduction, 21, 323-330, doi: 10.1016/j.ijdrr.2016.12.016.

Susilo, Meilano, I., Daryono, Efendi, J., Sarsito, D.A. & Basuki, A.Y., 2019. Preliminary coseismic deformation associated with the July 7th 2019 M 7.0 North Maluku earthquake. IOP Conference Series Earth and Environmental Science, 389(1), 012030, doi: 10.1088/1755-1315/389/1/012030.

Tanioka, Y., Miranda, G.J.A., Gusman, A.R. & Fujii, Y., 2017. Method to determine appropriate source models of large earthquakes including tsunami earthquakes for tsunami early warning in Central America. Pure and Applied Geophysics, 174, 3237-3248, doi: 10.1007/s00024-017-1630-y.

Thingbaijam, K.K.S., Mai, P.M. & Goda, K., 2017. Scaling relations of earthquake source parameter estimates with special focus on subduction environment. Bulletin of the Seismological Society of America, 107(5), 2225-2246, doi: 10.1785/0120100111.

Titov, V.V., 2021. Hard lesson of the 2018 Indonesian tsunamis. Pure and Applied Geophysics, 178, 1121-1133, doi: 10.1007/s00024-021-02731-0.

Triyoso, W., Suwondo, A., Yudistira, T. & Sahara, D.P., 2020. Seismic Hazard Function (SHF) study of coastal sources of Sumatra Island: SHF evaluation of Padang and Bengkulu cities. Geoscience Letters, 7(1), 1-7, doi: 10.1186/s40562-020-00151-x.

van Gorsel, J. T., 2018. Bibliography of the geology of Indonesia and surrounding areas: Java, Madura, Java Sea, 7.0, 1-297.

Walker, K.T., Ishii, M. & Shearer, P.M. 2005. Rupture details of the 28 March 2005 Sumatra Mw 8.6 earthquake imaged with teleseismic P waves. Geophysical Research Letters, 32(L24303), doi: 10.1029/2005GL024395.

Watkinson, I.M. & Hall, R., 2017. Fault systems of the eastern Indonesian triple junction: evaluation of Quaternary activity and implications for seismic hazards. In: Cummins, P.R. & Meilano, I. (Eds.), Geohazards in Indonesia: Earth Science for Disaster Risk Reduction. Geological Society of London: Special Publications, 441, 71-120, doi: 10.1144/SP441.8.

Wells, D.L. & Coppersmith, K. J., 1994. New empirical relationships among magnitude, rupture length, rupture width, rupture area, and surface displacement. Bulletin of the Seismological Society of America, 84(4), 974-1002.

Widiyantoro, S., Gunawan, E., Muhari, A., Rawlinson, N., Mori, J., Hanifa, N.R., Susilo, S., Supendi, P., Shiddiqi, H.A., Nugraha, A.D. & Putra, H.E., 2020. Implications for megathrust earthquakes and tsunamis from seismic gaps south of Java Indonesia. Scientific Reports, 10, 15274, doi: 10.1038/s41598-020-72142-z.

Wu, W.N., Zhao, L. & Wu Y.M., 2013. Empirical relationships between aftershock zone dimensions and moment magnitude for plate boundary earthquakes in Taiwan. Bulletin of the Seismological Society of America, 103(1), 424-436, doi: 10.1785/0120120173.

Xu, W., 2017. Finite-fault slip model of the 2016 M_w 7.5 Chiloé earthquake, southern Chile, estimated from Sentinel-1 data. Geophysical Research Letters, 44(10), 4774-4780, doi: 10.1002/2017GL073560.

Yen, Y.T. & Ma, K.F., 2011. Source-scaling relationship for M 4.6-8.9 earthquakes, specifically for earthquakes in the collision zone of Taiwan. Bulletin of the Seismological Society of America, 101(2), 464-481, doi: 10.1785/0120100046.

Manuscript received 10 May 2021;
Received in revised form 23 August 2021;
Accepted 27 September 2021
Available online 20 May 2022